Sediment clues in flood mitigation: the key to determining the origin, transport, and degree of heavy metal contamination

K. V. Annammala, N. A. Mohamad, D. Sugumaran, L. S. Masilamani, Y. Q. Liang, M. H. Jamal, Z. Yusop, A. R. M. Yusoff and A. Nainar

ABSTRACT

This study seeks to identify sediment sources, quantify erosion rates, and assess water quality status via sediment fingerprinting, the Modified Laser Erosion Bridge (MLEB) method, and various pollution indices (PIs), respectively, in the humid tropics (Malaysia). Geochemical elements were used as tracers in sediment fingerprinting. Erosion rates were measured at 3,241 points that encompass high conservation value forests (HCVFs); logged forests (LFs); mature oil palm (MOP); and mature rubber (MR) plantations. Annual erosion rates were 63.26–84.44, 42.38, 43.76–84.40, and 5.92–59.32 t ha^{-1} yr^{-1} in the HCVF, LF, MOP, and MR, respectively. Via sediment fingerprinting, logging and agricultural plantations were identified as the major contributors of the sediment. PIs also indicated the highest level of pollution in those catchments. This study highlighted three main messages: (i) the feasibility and applicability of the multiproxy sediment fingerprinting approach in identifying disaster-prone areas; (ii) the MLEB as a reliable and accurate method for monitoring erosion rates within forested and cultivated landscapes; and (iii) the adaptation of PIs in providing information regarding the status of river water quality without additional laboratory analyses. The combination of these approaches aids in identifying high-risk and disaster-prone areas for the prioritisation of preventive measures in the tropics.

Key words | erosion, land-use, oil palm, plantation, pollution, sediment fingerprinting

HIGHLIGHTS

- Sediment fingerprinting identified modifies landscapes and a major contributor of sediment in the tropics.
- High erosion found in various tropical catchments such as in forests, rubber, and oil palm plantations.
- Sediment pollution indices are useful and practical in indicating the health of a catchment system.

K. V. Annammala (corresponding author)
Z. Yusop
Centre of Environmental Sustainability & Water Security (IPASA), Research Institute for Sustainable Environment (RISE), Universiti Teknologi Malaysia,
Johor,
Malaysia
E-mail: *kogila@utm.my*

K. V. Annammala
N. A. Mohamad
D. Sugumaran
L. S. Masilamani
Y. Q. Liang
Z. Yusop
Department of Water and Environmental Engineering, School of Civil Engineering,
Universiti Teknologi Malaysia,
Johor,
Malaysia

M. H. Jamal
Centre for Coastal and Ocean Engineering (COEI),
Universiti Teknologi Malaysia,
Johor,
Malaysia

A. R. M. Yusoff
Department of Chemistry, Faculty of Science,
Universiti Teknologi Malaysia,
Johor,
Malaysia

A. Nainar
Ecohydrology Research Institute, The University of Tokyo Forests, Graduate School of Agricultural and Life Science, The University of Tokyo,
Aichi,
Japan

doi: 10.2166/nh.2020.119

INTRODUCTION

Over the past decade, several countries have experienced devastating and catastrophic flooding events, including the Yangtze River in China, the Mekong River in Vietnam, the Vistula River in Poland, and the Brisbane River in Australia, and the Marikina River in Philippines (Li *et al.* 2016). One of the worst flood events ever recorded in the history of Malaysia was the north-east coast flood in the state of Kelantan between December 2014 and January 2015. During this period, over 200 thousand people were evacuated from their homes to higher grounds. This flood was also known as the 'Big Yellow Flood' because of the murky water that carried large amounts of sediment (Alias *et al.* 2016).

Generally, sedimentation plays a significant role in the development and maintenance of hydrological and biological habitats of a fluvial system including lagoons, estuaries, wetlands, sand barriers, dunes, mangroves, and coral reefs (Varol & Bülent 2012). According to Dedkov & Gusarov (2006), the estimated global sediment flux from major rivers of the world into the ocean is 15.5×10^9 t yr^{-1}, of which approximately 74% is supplied from Asia and the Pacific islands.

Sediment serves as a dominant sink for various contaminants especially hazardous heavy metals (Varol & Bülent 2012; Pejman *et al.* 2015). Heavy metals are diffused through the freshwater environment by both natural processes (e.g., rock weathering, soil erosion, and volcanic eruption) and anthropogenic activities (e.g., mining, industrial and urban wastewater discharges, and agricultural runoff) (Pejman *et al.* 2015). Varol & Bülent (2012) stated that up to 98% of heavy metals entering a river can be stored or deposited in the sediment through adsorption and precipitation processes. Since these heavy metals have longer residence time in sediments, they can easily bio-accumulate in the tissues of aquatic species, which may affect the distribution and diversity of benthic organisms living in contact with the sediment (Varol & Bülent 2012; Pejman *et al.* 2015). Sediment also acts as a secondary source of pollution where it may release sediment-bound heavy metals back into the water column during changes in environmental conditions (e.g., pH and temperature) (Varol & Bülent 2012). Therefore, sediment contamination by heavy metals indicates serious deterioration of the health of a freshwater environment. Nevertheless, sediment redistribution within a fluvial system is a complex process. Thus, transportation and deposition rates are highly influenced by sediment yield within a watershed (Tundu *et al.* 2018), affecting even downstream reaches by making them more prone to flood risk due to changes in channel stability and river depth.

Land conversion-related activities alter slope topography, soil properties, and vegetation cover, hence accelerating the soil erosion process. Hillslopes are being modified for agricultural purposes in both temperate and tropical regions; and, in Malaysia, oil palm plantations have reached 5.90 million ha as of 2019, that is a 0.9% increase from the previous year (5.85 million ha) (MPOB 2020). Meanwhile, in Peninsular Malaysia, approximately 74 thousand ha of forested area were converted into new timber latex clone rubber plantation between 2005 and 2009 (Lim 2013).

Substantial disturbances on the soil surface greatly accelerate erosion rates by 10–100-fold and thus contribute to higher suspended sediment concentrations compared with natural, undisturbed catchments (Nainar *et al.* 2017). In times of high rain intensity, uncovered ground surfaces are directly impacted by large raindrops with high momentum, consequently accelerating the soil particle detachment and resulting in higher sediment (erosion) transported via overland flow. This erosion becomes more severe as overland flow channelises to form rills and gullies. This process contributes to increased sedimentation rates, therefore increasing the probability of sediment deposition in reservoirs and riverbeds, causing floods.

Frequent flood catastrophes can have devastating consequences including disease outbreaks, casualties, property, and crop damage, affecting both the socio-economy and natural environment of a nation. As an example, the massive flood in Kelantan had caused the deaths of 12 people, over RM2.8 billion in material losses, and left more than 1,600 residents homeless. Climate change may have played a significant role in the recurrence of flood in Kelantan (Alias *et al.* 2016). However, only limited studies have highlighted the impacts of land-use changes on floods (Annammala *et al.* 2018; Nainar *et al.* 2018).

In Malaysia, especially in the state of Kelantan, active land conversion into agricultural plantations as well as logging have been reported to cause high levels of sedimentation downstream. Large-scale land clearance and conversion accelerate sedimentation in a river system, eventually resulting in floods especially during the monsoon periods.

This paper addresses the issues highlighted above and aims to identify the origin of downstream sediments within a large catchment via the environmental forensics approach. This study also identifies disaster-prone areas within a large catchment that may aid mitigation plans.

The main themes addressed in this paper included:

1. Methods to identify the origin of the large catchment scale sediment through the sediment fingerprinting technique using the Kelantan River Basin (KRB) in Malaysia as the research setting.
2. Determining and comparing accelerated erosion rates across a gradient of forest disturbances. To determine the magnitude of erosion within a disturbed forest, mature oil palm and rubber plantation sites (the major land-uses in Malaysia and most parts in southeast Asia).
3. Assessing the degree of heavy metal contamination within the study area using multiple sediment pollution indices (PIs).

The results presented in this paper are from a combination of a field experiment, mathematical models, statistical analyses, and an adaptation of multiple sediment pollution indices. The approaches and methods reported here can be replicated to initiate targeted flood control measures in tropical regions.

STUDY AREA

The KRB is the main river that flows through the state of Kelantan, located in West Malaysia (4–6°N latitude and 101–103°E longitude). The length of the river is approximately 248 km, and it is divided into two main channels – the Lebir and Galas River as shown in Figure 1. The merging

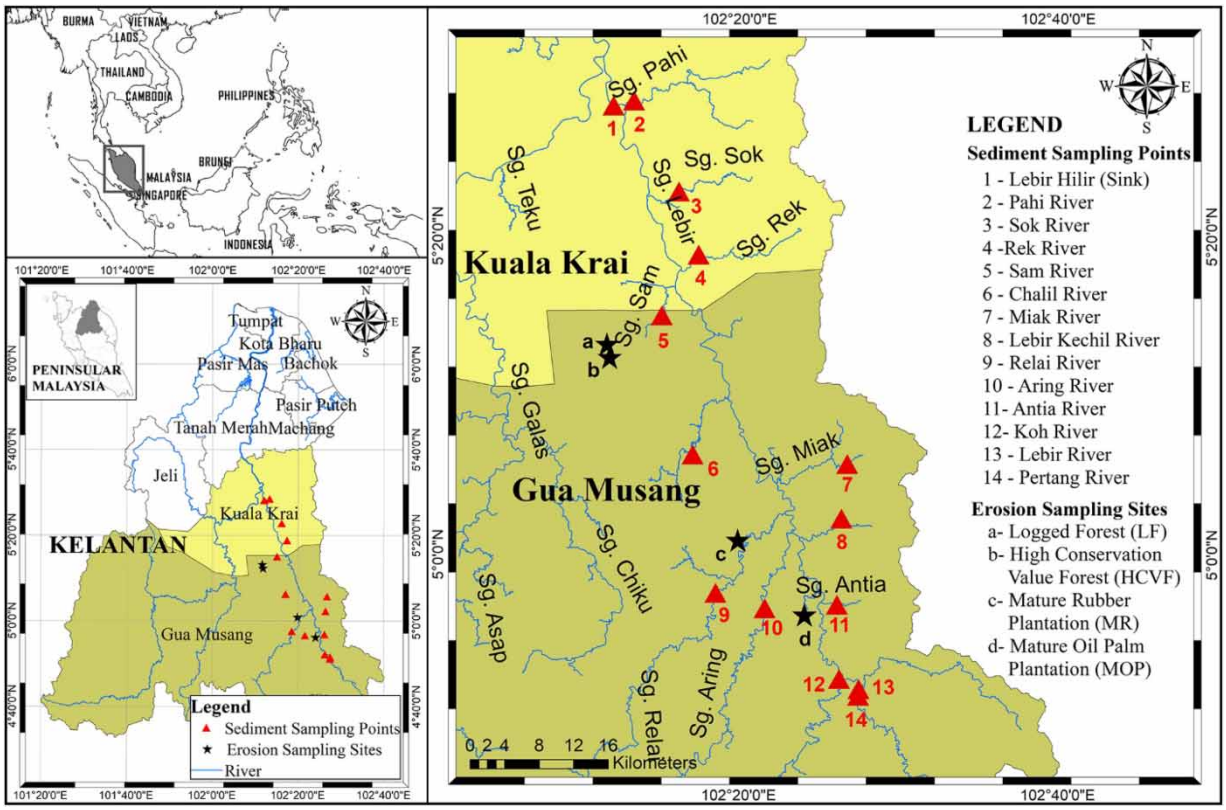

Figure 1 | The study area.

point of these two rivers is near Kuala Krai, which is about 100 km from the estuary. The climate of KRB is tropical equatorial characterised by heavy rainfall throughout the year. The annual precipitation of approximately 2,500 mm influenced by the northeast monsoon (mid-October to mid-January) is common (Hydrology and Water Resources Research Laboratory Kyoto University 2018). The Lebir catchment covers approximately 2,500 km^2 of drainage area with oil palm cultivation, rubber plantations, and paddy fields as its major land-uses within the basin. Besides these, timber harvesting and mining are also actively being practised in some parts of this catchment. The geology is dominated by a melange of acid intrusive rocks, Permian sedimentary rocks (slate, phyllites, sandstone, and limestone), and Triassic sedimentary rocks (shale, siltstone, sandstone, and limestone) (Hydrology and Water Resources Research Laboratory Kyoto University 2018).

MATERIAL AND METHODS

Sediment source sampling

Riverbank sediment samples were collected during the dry season in the middle of March 2018. The sediment source sampling procedure involved the collection of surface and subsurface materials along the riverbank at depths of 0–3 cm and below 3 cm, respectively. A total of 84 surface and subsurface soil samples were collected from 14 tributaries feeding into the Lebir catchment (Figure 1). Fine fractions (less than 63 μm) were analysed using a benchtop NEXCG ED X-Ray Fluorescent (XRF). The sediment fingerprinting analysis and statistical methods used were as reported in Annammala *et al.* (2018). A multivariate unmixing model via the Microsoft Excel solver command was used to calculate the relative sediment mixing proportions in the KRB.

Erosion rate measurement

Soil erosion rates were monitored for 24 months (March 2017–February 2019) at four sites – corresponding to the land-uses within the KRB. The investigated land-uses comprise a high conservation value forest (HCVF), logged forest (LF), mature oil palm plantation (MOP), and mature rubber plantation (MR) (Figure 1). Palm trees are considered to be mature and productive 3 years after planting; and rubber, 7 years after planting. Soil erosion was measured using the Modified Laser Erosion Bridge (MLEB) technique (Annammala *et al.* 2012; Mohamad *et al.* 2018). Net changes in ground height (erosion or deposition) were measured at 3-month intervals (at times, 5-month intervals when accessibility is poor). Measurements were divided into four phases: phase I (March–July 2017), phase II (August 2017–February 2018), phase III (March–July 2018), and phase IV (August 2018–February 2019). Over 108 erosion transects were set up, which enabled 3,239 measurements of ground height change (GHC). Each point was measured by means of a laser distance meter. The accuracy of measurement was reported at <1.1 mm, as tested by Annammala *et al.* (2012). During measurement, it was noted as to whether the ground was covered with leaf litter (LL), undergrowth, organic matter/surface roots (OM), loose soil (LS), small stones (SS), woody debris (WD), bare ground (BG), or root networks (R). In addition, any occurrence of split laser beams (SBs) due to uneven soil surface was noted. These were important observations in explaining the nature of the observed GHC. In cases where thick LL, OM, WD, or R covers were found, the obstacles were carefully moved aside to measure the soil surface and then returned to their original position after measurement. Ground-lowering rates in the study area were converted to the erosion rate (ER) in tonnes-per-ha-per-year using the equation:

$$\mathrm{ER}\,(\mathrm{t\,ha^{-1}\,yr^{-1}}) = 10\,\mathrm{BD} \times \mathrm{GL} \quad (1)$$

where BD is the bulk density in g cm^{-3} and GL is the ground-lowering rates in mm yr^{-1} (Clarke & Walsh 2006). The mean soil bulk densities (g cm^{-3}) used to convert GHC to the erosion rate were 0.91, 0.84, 1.26, and 1.18 g cm^{-3} for HCVF, LF, MOP, and MR, respectively.

Assessment of sediment contamination

Sediment-related PIs are essential tools in evaluating the level of trace metal contamination in river sediment. The current study focused on the geo-accumulation index (I_{geo}) (Muller 1969), potential ecological risk index (RI)

(Hakanson 1980), background enrichment factor (PIN) (Caeiro *et al.* 2005), and modified contamination degree (mCd) (Abrahim & Parker 2008). Considering that pre-industrial-age elemental concentration data for the study area are not available, the average values for shale provided by Turekian & Wedepohl (1961) were used as background concentrations to assess the sediment contamination level.

Geo-accumulation index (I_{geo})

I_{geo} was used to assess anthropogenic impact via the following equation:

$$I_{geo} = \log_2 (C_n/1.5B_n) \quad (2)$$

where C_n is the metal concentration in the sediment, B_n is the background concentration of the element (average values for shale), and the factor 1.5 is the compensating factor for the background data due to the lithogenic effect. Muller (1969) classified the I_{geo} into seven main classes, as shown in Table 1.

Modified contamination degree (mCd)

Abrahim & Parker (2008) proposed the usage of mCd to evaluate the overall heavy metal contamination.

$$\mathrm{mCd} = \frac{\sum_{i=0}^{i=n} \mathrm{CF}}{n} \quad (3)$$

$$\mathrm{CF} = \frac{C^i_{\mathrm{sample}}}{C^i_{\mathrm{ref}}} \quad (4)$$

Table 1 | Classes of geo-accumulation index (I_{geo})

Class	I_{geo} values	Level of contamination
0	$I_{geo} \leq 0$	Uncontaminated
1	$0 < I_{geo} \leq 1$	Uncontaminated to moderately contaminated
2	$1 < I_{geo} \leq 2$	Moderately contaminated
3	$2 < I_{geo} \leq 3$	Moderately to strongly contaminated
4	$3 < I_{geo} \leq 4$	Strongly contaminated
5	$4 < I_{geo} \leq 5$	Strongly to extremely contaminated
6	$I_{geo} > 5$	Extremely contaminated

where CF is the contamination factor, C^i_{sample} is the measured value of the heavy element in the sediment, C^i_{ref} is the average concentration for shale, and n is the number of the analysed elements. PLI values were categorised into three main classes: $\mathrm{mCd} < 1.5$ (uncontaminated); $1.5 \leq \mathrm{mCd} < 2$ (low degree of contamination); $2 \leq \mathrm{mCd} < 4$ (moderate degree of contamination); $4 \leq \mathrm{mCd} < 8$ (high degree of contamination); $8 \leq \mathrm{mCd} < 16$ (very high degree of contamination); $16 \leq \mathrm{mCd} < 32$ (extremely high degree of contamination); $\mathrm{mCd} \geq 32$ (ultra-high degree of contamination).

Potential ecological risk index (RI)

The RI, proposed by Hakanson (1980), was designed to evaluate the potential risk of heavy metal poisoning for freshwater organisms. The RI is calculated using the following formula:

$$\mathrm{RI} = \sum_{i=0}^{n} E^i_r = \sum_{i=0}^{n} T^i_r \times C^i_f \quad (5)$$

where E^i_r and T^i_r are the potential ecological risk factor and toxic response factor, respectively, for the given element, i. The toxic response factors for Pb, As, Ni, Cu, Cr, Zn, Mn, and Co are 5, 10, 5, 5, 2, 1, 1, and 5, respectively (Hakanson 1980). C^i_f is the contamination factor (Abrahim & Parker 2008). RI values were categorised into four classes: $\mathrm{RI} < 150$ (low ecological risk); $150 \leq \mathrm{RI} < 300$ (moderate ecological risk); $300 \leq \mathrm{RI} < 600$ (considerable ecological risk); and $\mathrm{RI} > 600$ (very high ecological risk).

Background enrichment factor (PIN)

Caeiro *et al.* (2005) introduced the PIN to assess the enrichment trace metals in sediment using the class of contamination factor. The PIN is computed using the following equation:

$$\mathrm{PIN} = \sum_{i=0}^{n} \frac{w_i^2 \times c_i}{\mathrm{GB}} \quad (6)$$

where w_i is the class of the contamination factor of the ith metal, C_i is the concentration of the ith metal, and GB is

the geochemical background concentration (average value for shale). Caeiro *et al.* (2005) classified PIN values into five main classes, as shown in Table 2.

RESULTS AND DISCUSSION

Sediment fingerprinting results: sediment source ascriptions

Optimum fingerprinting properties

The optimisation of elemental selection was carried out using statistical analysis, which involved a non-parametric Kruskal–Wallis *H* test followed by a stepwise discriminant function analysis (DFA). The Kruskal–Wallis *H* test failed to reject the null hypothesis for five elements ($p > 0.05$) (Table 3), thereby indicating no significant difference in elemental concentration among the various sources. Next, a stepwise DFA was applied to select an optimal set of tracers via the elimination of redundant tracers from the selected fingerprint properties. In other words, DFA performed a competency analysis to predict group-association on the basis of the means of the variables. The DFA selected a combination of 10 tracer properties (Mn, Ti, Ca, Cr, Ba, Eu, Gd, Cu, Fe, and Pb) as the best signatures of the sources based on the minimisation of Wilks' lambda and highlighting elements with high discriminatory power in relation to the source areas in the catchment. Elements with *F*-values that fall within the range to be included in the analysis (2.71–3.84) are shown in Table 4. Overall, 97% of the sediment sources were classified into respective groups. The output from the Wilks' lambda test indicated differences among the means from the multiple sources (Table 4).

Selected geochemical elements could be classified into three major groups, namely alkaline earth metals (Ca and Ba), transition metals (Mn, Ti, Cr, Fe, Cu, and Pb), and lanthanide elements (Eu and Gd). This classification shows that Earth crust metals were the dominant elements in the current findings. Mean concentrations of the geochemical tracers were compared with that in other sites and in the sink areas (coloured red in Figure 2). The boxplots in Figure 2(a) represent the mean concentration of the sink and sources of the element manganese (Mn). Mn is a frequently detected element in soils/sediments and originates from rock weathering, atmospheric deposition, and oxidation reactions in the soil (Nádaská *et al.* 2010). It was observed that the Miak River (source 7) with a mean concentration between 1,250 and 2,770 ppm fell within the range of values of the sink. In contrast, other sources were lower in terms of concentration range when compared with the sink except for in the Aring River where Fe concentrations were of a wider range (44,000–73,000 ppm) (Figure 2(b)). Fe is also an Earth crust metal and could be enriched due to anthropogenic activities such as iron ore mining. The sources that fell within the range of sink concentrations were the Sok River (44,900–179,000 ppm),

Table 2 | Classes of background enrichment factor (PIN)

Class	PIN values	Level of contamination
1	$0 < \text{PIN} \leq 7$	Clean
2	$7 < \text{PIN} \leq 95.1$	Trace contamination
3	$95.1 < \text{PIN} \leq 518.1$	Lightly contaminated
4	$518.1 < \text{PIN} \leq 2{,}548.6$	Contaminated
5	$\text{PIN} > 2{,}548.6$	Highly contaminated

Table 3 | The output of non-parametric Kruskal–Wallis *H* test for each source tracer

Tracer	*H*-value	*p*-Value
Na	28.02	0.01*
Mg	20.23	0.063
Ca	34.46	0.00*
Ti	33.01	0.00*
V	29.86	0.00*
Cr	29.79	0.00*
Mn	35.78	0.00*
Fe	29.64	0.00*
Co	17.32	0.138
Ni	25.53	0.01*
Cu	27.54	0.01*
As	17.62	0.128
Kr	15.79	0.201
Ba	31.72	0.00*
Pb	35.60	0.00*
Eu	26.78	0.01*
Gd	36.48	0.00*
Tb	20.16	0.064

*Statistically significantly different at $p < 0.05$.

Table 4 | The optimum number of tracer selected by the stepwise DFA

Variable entered/removed[a,b,c,d]

						F-value			
Step	**Element**	**Statistic**	**df1**	**df2**	**df3**	**Statistic**	**df1**	**df2**	**df3**
1	Mn	0.002	1	12	26	962.13	12	26	0
2	Ti	0	2	12	26	220.57	24	50	0
3	Ca	0	3	12	26	114.801	36	71.64	0
4	Cr	0	4	12	26	70.375	48	90.64	0
5	Ba	0	5	12	26	54.777	60	106.8	0
6	Eu	0	6	12	26	43.862	72	120.1	0
7	Gd	0	7	12	26	36.754	84	130.5	0
8	Cu	0	8	12	26	34.567	96	138.3	0
9	Fe	0	9	12	26	30.991	108	143.6	0
10	Pb	0	10	12	26	28.024	120	146.7	0

1. The shown *F*-values for all steps are approximated with exception to steps 1 and 2 that are exact *F*-values.
2. At each step, the variable that minimises the overall Wilks' lambda is entered.
a. Maximum number of steps is 26.
b. Minimum partial *F* to enter is 3.84.
c. Maximum partial *F* to remove is 2.71.
d. F level, tolerance, or VIN insufficient for further computation.
3. The classification output shows 97.4% of original grouped cases correctly classified.

Sam River (46,300–55,700 ppm), Relai River (48,600–55,400 ppm), Antia River (56,700–77,100 ppm), and Pertang River (64,400–69,900 ppm). The concentration of sources in the Chalil, Miak, Lebir Kechil, and Aring rivers (89,900; 68,900; 76,900; and 61,900 ppm, respectively) was higher than that in the sinks, whereas other rivers have source concentrations that fell below that of the sink. Meanwhile, for elements Eu and Gd, the mean concentration of the sinks ranged 670–350 and 310–460 ppm, respectively. As for Eu, two rivers, namely the Sok (Source 3) and Chalil (Source 6), have concentrations that were within the sink value with mean concentrations of 237–1,000 and 285–1,620 ppm, respectively. In general, concentrations of elements in source areas fell below that in sink areas except for in the Aring River (source was 3,700 ppm higher than in sink). For the element Gd, only one source was within the range of its sink value, that is the Lebir Kechil River (425–860 ppm). Sources in three rivers, namely the Chalil River, Miak River, and Aring River, had concentration values higher than those in their sinks while the other rivers were all below the detection limit (BDL). In Figure 2(e), element Ti has a smaller range (8,300–9,400 ppm) than the sink value; thus, only three sources (Chalil, Lebir, and Koh) fell within the mean concentration of the Lebir–Hilir sink. Concentrations of the other detected elements with respect to the sinks area are presented in Figure 2.

Beside mean concentrations visualised in boxplots, output from the DFA (Figure 3) with unique group centroid clustering was also produced. Sites that have a history of mining activity showed distinctive clustering characteristics compared with other land-uses (Table 5). Heavily disturbed catchments with active land clearance where oil palm plantations exist tend to cluster closer together. Also, an actively logged sub-catchment that includes an oil palm plantation was observed to have distinct properties compared with other catchments with a mixture of land disturbances. Tropical regions are known for their complex combination of soil classification and mixed vegetation cover which could be a reason behind the observed co-clustering effect.

Sediment source apportionment

The sediment fingerprinting approach for identifying sediment sources and their relative contribution to the

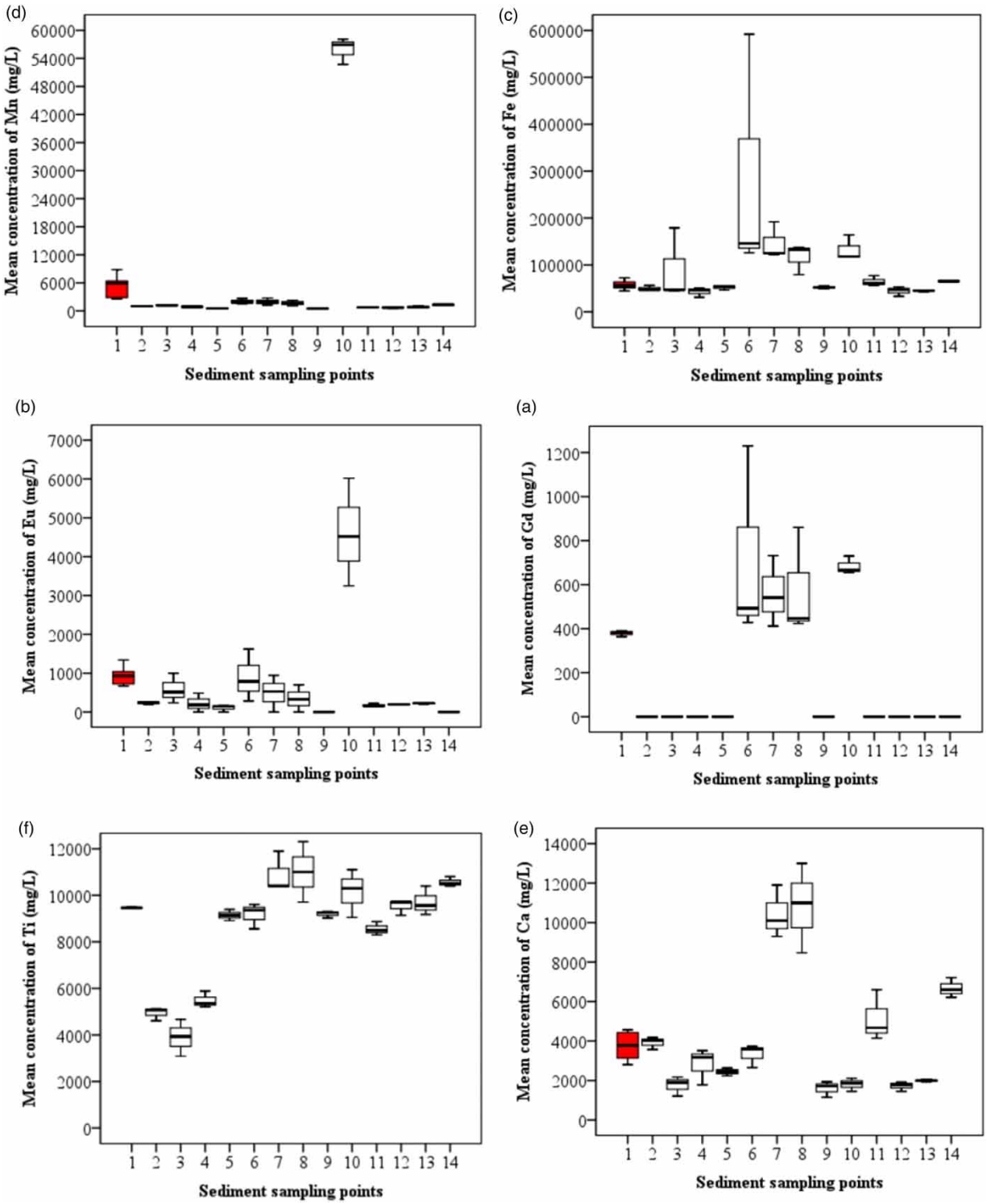

Figure 2 | The boxplots of the selected geochemical signatures with boxes in red representing the sinks. (a) Manganese (Mn), (b) Iron (Fe), (c) Europium (Eu), (d) Gadolinium (Gd), (e) Titanium (Ti), (f) Calcium (Ca), (g) Chromium (Cr), (h) Copper (Cu), (i) Lead (Pb), and (j) Barium (Ba). Please refer to the online version of this paper to see this figure in colour: http://dx.doi.10.2166/nh.2020.119. *(Continued.)*

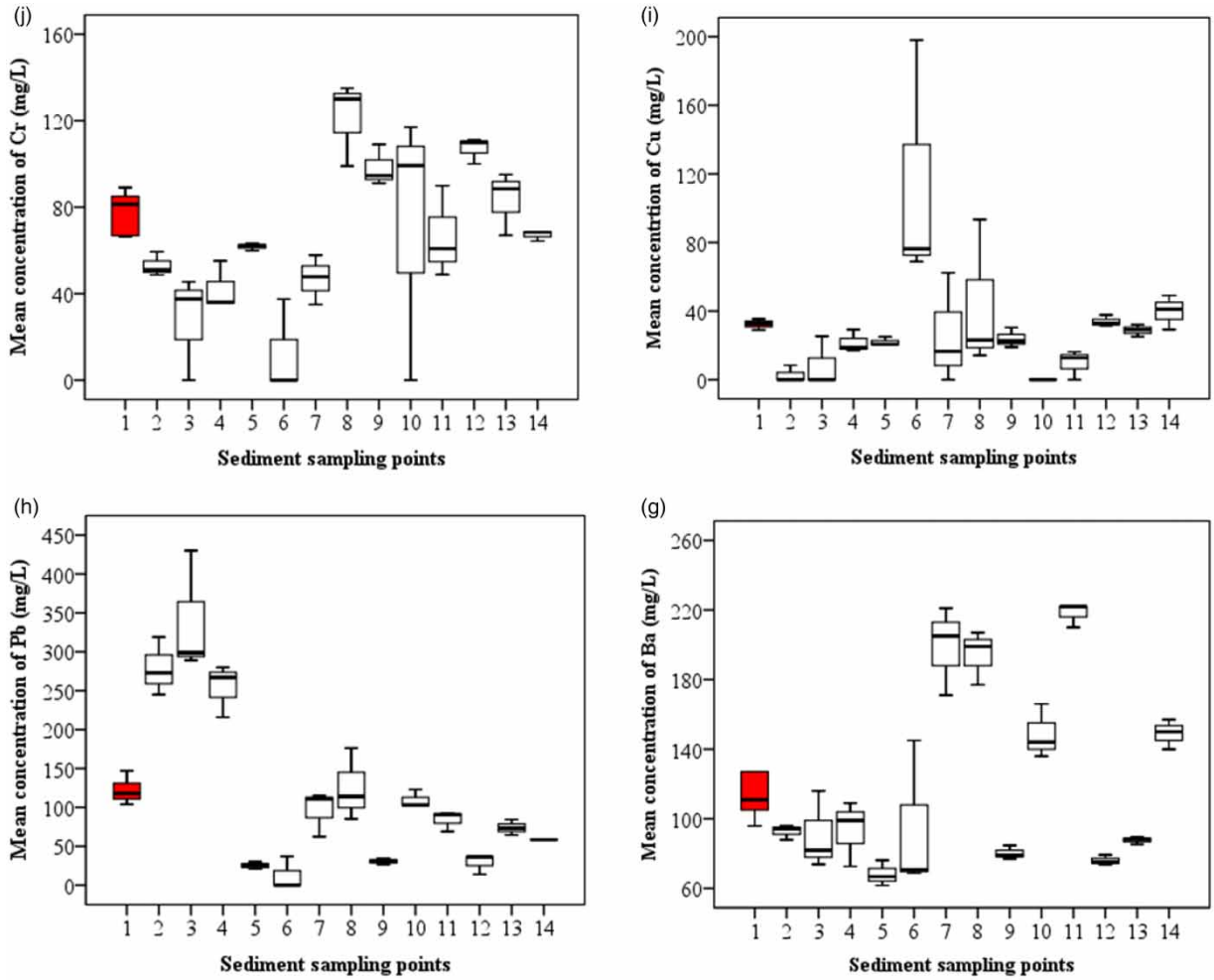

Figure 2 | Continued.

catchment system is one of the main objectives of this investigation and is achieved through the application of the multivariate unmixing model (Walsh *et al.* 2011; Annammala *et al.* 2018) (Figure 4).

Results suggested that the Lebir Kecil River is the major contributor of sediment to the Lebir catchment – up to 27%. This high sediment contribution can be related to anthropogenic activities that were taking place within the subcatchment. Observation using Google Maps 2019 indicated an active oil palm plantation region. Additionally, based on field observations, oil palm was planted at the edge of the riverbank in some estates. Riverbanks such as these are usually classified as sensitive areas and should be protected by riparian reserves (Luke *et al.* 2017). This may be one of the contributing factors to the accelerated sedimentation rate especially during replanting periods and the monsoon season. The second major sediment contributor to the catchment is the Lebir River, followed by the Sok, Koh, Aring, Chalil, and Miak rivers with contributions of 21, 16, 13, 10, 10, and 3%, respectively. The Kelantan land-use map from the years 2010 and 2013 were used to validate the results.

The Lebir and Koh rivers primarily originate upstream of the Kuala Koh National Park (catchment sizes approximately 45 and 146 km^2, respectively). This region is classified as protected forest area and, geographically, is of

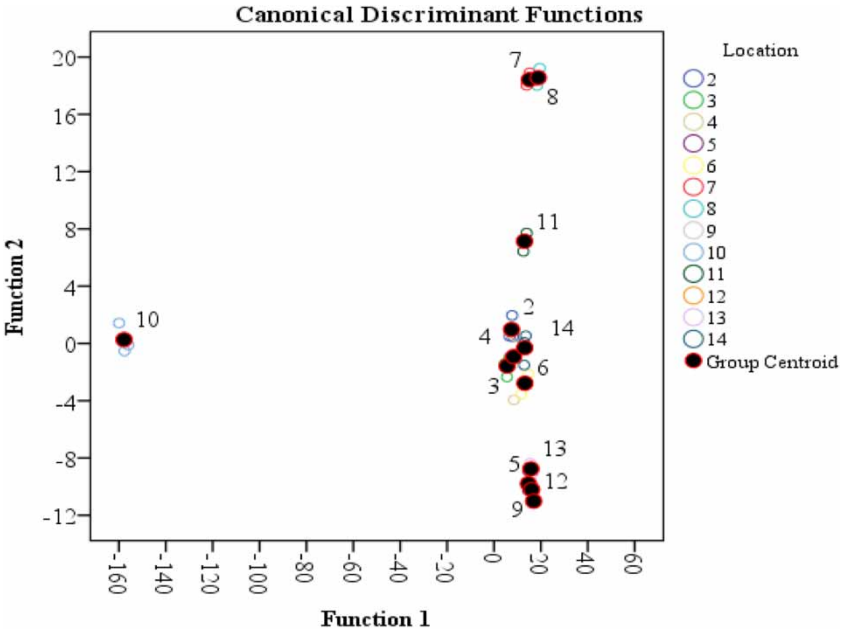

Figure 3 | The output of DFA on land-use classification for the Lebir catchment.

Table 5 | Catchment size and land-use of sampling points

No.	Location	Catchment size (km^2)	Major land-use activities
1	Lebir Hilir	28	Sink
2	Pahi	109	Oil palm and rubber plantations + land clearance[a]
3	Sok	115	Rubber plantation
4	Rek	96	Rubber plantation
5	Sam	20	Rubber and oil palm plantations + land clearance[a]
6	Chalil	46	Rubber plantations + oil palm plantations
7	Miak	63	Oil palm plantations + land clearance[a]
8	Lebir Kecil	105	Oil palm plantations + land clearance[a]
9	Relai	475	Oil palm plantations
10	Aring	436	Oil palm plantations + mining
11	Antia	34	Oil palm plantation + logging
12	Koh	146	Forest region
13	Lebir	46	Forest region
14	Pertang	173	Forest region

[a]Land clearance for new plantation site.

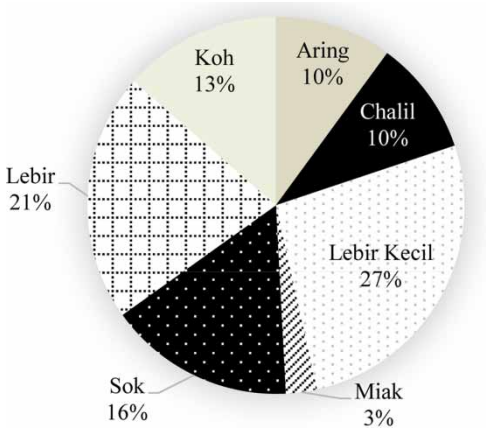

Figure 4 | The relative sediment contribution from various sources into the Lebir River of the KRB.

moderate to high in terms of elevation (350–550 m above sea level). Yet, both of these sources show high contribution of sediment within the large KRB system. The cause for this is unknown although anthropogenic activities such as land clearing and mining may have played a role, but this hypothesis requires further investigation. It has also been reported that when the headwaters of a catchment are disturbed, an

increase in the sedimentation rate can be observed throughout the catchment (more intensive downstream) (Walsh *et al.* 2011). In the Sok sub-catchment, rubber plantations are the dominant agricultural activity. It can be observed that this sub-catchment has been subjected to large-scale land clearance and is still actively being converted into agricultural plantations. Dredging activity in this part of the river was also observed during the sediment sampling period. Anthropogenic activities can greatly affect land stability and induce higher sedimentation rates. The combination of all these factors could be the cause behind the strong signal of sediment contribution from this part of the catchment. Targeted erosion and sediment control plans (ESCPs) can therefore be initiated in the identified high-contribution areas. However, a general ESCP may not be applicable to all sites because some sites require riparian zone allocations, while others will require cover crop or other means. Prescribing suitable treatments will require further works with all stakeholders, which, for the case of Malaysia, will include landowners, the local authority, engineers, and environmental consultants.

Meanwhile, the Aring and Chalil sub-catchment showed a similar proportion of sediment contribution to the Lebir catchment. Both of these rivers with catchment sizes of around 435 and 184 km^2, respectively, were dominated by oil palm plantations. Forest-clearing and oil palm expansion began in the 1980s under the Federal Land Development Authority (FELDA) project and settlement scheme. Since then, plantations and crop production have been active and land clearing has continued to take place. In addition, soils in these regions are mostly dominated by silt and clay which can be easily redistributed during periods of high rainfall or when anthropogenic activities take place. Similarly, the Miak River is highly susceptible to high sedimentation due to active land clearance for plantation establishment. Also, in the Aring catchment, iron ore mining activities have been ongoing, which explains the high concentration of Fe in the sediments – also a possible reason for the high sedimentation rate in this river channel. Other possibilities for the high erosion and sedimentation rates include sediment from exposed ground without vegetation cover. The uses of heavy vehicles and machinery in logging and road construction have also been reported to cause higher erosion and sedimentation (Walsh *et al.* 2011).

Soil erosion

Changes in ground height

Over 3,239 *in situ* measurements were obtained. Erosion data are represented by negative (−) and positive (+) numbers indicating erosion and deposition, respectively. Table 6 shows the mean GHC rates and total rainfall at each location. The mean values delineate towards negative changes (erosion) during all monitoring phases. Measured GHC values in forested areas (HCVF and LF) showed mean erosion values throughout all phases. The highest GHC (erosion) values recorded in HCVF and LF were 6.14 and 3.58 mm, respectively, during phase II. Total rainfall recorded during this period was 1,662 mm. Both agricultural plantations (MOP and MR) recorded net erosion in phases I, II, and IV. In phase III, net depositions of 0.28 mm in MOP and 0.61 mm in MR were recorded, with total rainfall of 1,027 mm. In MOP and MR, GHC is the highest (net erosion) in phase IV at 7.50 and 5.68 mm, respectively, albeit having slightly lower total rainfall (1,516 mm) compared with that in phase II (1,604 mm). From the overall field observation and measurements, the most critical erosion was observed during August 2017 to February 2018 and August 2018 to February 2019.

Results indicated that the months from August to February (phases II and IV) generated the most GHC which may be linked to the northeast monsoon from November to March – one of the two major monsoons experienced by southeast Asian countries (Alias *et al.* 2016). Erosion and sediment transport down the catchments are accelerated by raindrop impact on the ground surface followed by overland flow (Nainar *et al.* 2017; Mohamad *et al.* 2018). High rainfall intensity causes higher erosion rates within altered landscapes when best management practices (BMPs) are not in place (Duan *et al.* 2015), resulting in higher sedimentation and decreased depth in the river channel. This poses higher flood risk to riverbank areas and communities especially during extreme events.

Figure 5 shows the mean GHC pattern for the different land-uses over the four phases. Phases I, II, and IV had erosion, while phase III had deposition. Net erosion was recorded in phases I, II, and IV in all land-uses. In phase

Table 6 | Changes in mean ground height (mm) between March 2017 and February 2019 in the different land-uses

	Land-use practices								Total rainfall (mm)	
	HCVF		LF		MOP		MR			
Phase	GHC (SE)	*n*	GHC (SE)	*n*	GHC (SE)	*n*	GHC (SE)	*n*	HCVF and LF	MOP and MR
I	−2.26 (1.1)	450	−1.46 (0.8)	509	−2.39 (1.0)	810	−0.26 (0.3)	1,440	420	503
II	−6.14 (0.9)	450	−3.58 (1.0)	509	−1.09 (0.7)	810	−0.24 (0.4)	1,440	1,662	1,604
III	−5.92 (0.9)	480	No data		0.28 (0.6)	780	0.61 (0.5)	1,410	851	1,027
IV	− 3.36 (1.1)	480	No data		− 7.50 (0.7)	720	− 5.68 (0.5)	1,320	1,188	1,516

Phase: I = Mar.–July 17; II = Aug. 17–Feb. 18; III = Mar.–July 18; IV = Aug. 18–Feb. 19.
GL, mean ground-lowering level (mm) (negative, erosion; positive, deposition); SE, standard error; *N*, number of points.

III, net deposition was found in MOP and MR, while net erosion was found only in HCVF.

Soil erosion rates

HCVF showed have erosion rates between 63.26 and 84.44 t ha^{-1} yr^{-1} for periods 2017–2018 and 2018–2019, respectively (Table 7). Overall land-use sites indicated an increase in soil erosion rates for both time periods. MR experienced sharp increases in erosion rates of up to 82%, while MOP increased 32%, and HCVF increased 14%. The drastic increases in erosion rates recorded in MR and MOP may be related to increases in total annual rainfall from the first to the second year (as much as 436 mm), as there were no changes in land-use throughout the years. However, soil erosion rates in HCVF still increased 14% despite annual rainfall decreasing slightly from the first (2,082 mm) to the second year (2,039 mm). Figure 6 summarises the erosion dynamics.

Based on this observation, rainfall may be used to estimate erosion in the future, but more observation is required to develop a better rainfall–erosion relationship. Ultimately, the development of regional models may be preferred for the case of Malaysia, but the effects of other factors (slope gradient, geology, leaf area index, and aboveground biomass) need to be better understood. At least for

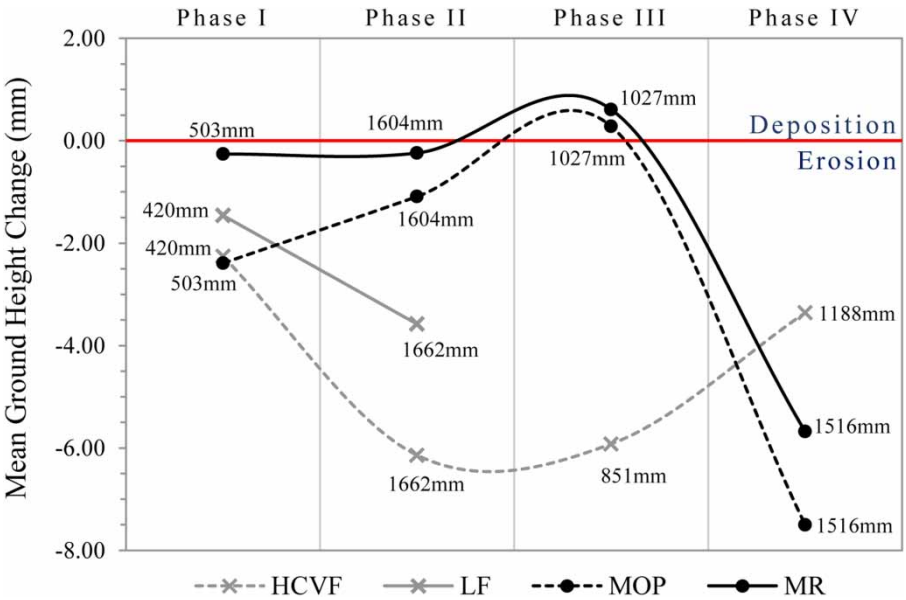

Figure 5 | Mean GHC for the different land-uses over the four phases. Numbers with the unit mm are total rainfall. Labels in the plot area are total rainfall.

Table 7 | Erosion rates t ha^{-1} yr^{-1} from 2017 to 2019

	Land-use practices								Total rainfall (mm)	
	HCVF		LF		MOP		MR			
Period	ER (SE)	*n*	ER (SE)	*n*	ER (SE)	*n*	ER (SE)	*n*	HCVF and LF	MOP and MR
2017–2018	−63.26 (10.6)	480	−42.38 (9.5)	509	−43.76 (12.6)	810	−5.92 (4.7)	1,440	2,082	2,107
2018–2019	−84.44 (10.2)	480	No data		−84.40 (8.9)	720	−59.32 (5.9)	1,320	2,039	2,543

ER, erosion rates (in t ha^{-1} yr^{-1}) (negative, erosion; positive, deposition); SE, standard error; *n*, number of points.

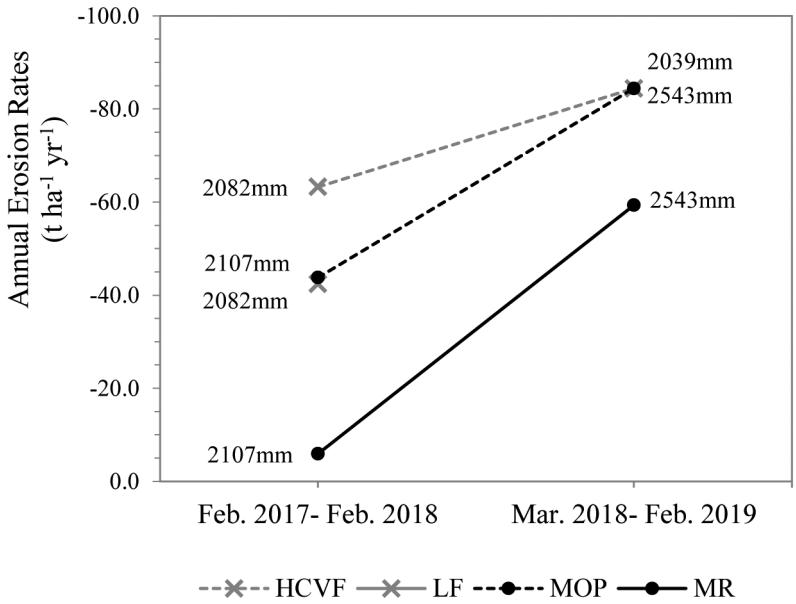

Figure 6 | Erosion dynamics and total rainfall for the different land-uses. Labels in the plot area are annual rainfall. The LF had only one data point.

the moment, results clearly indicate higher erosion rates in disturbed catchments. Installation of ESCPs has been suggested for these sites. In addition, the application of BMPs within agricultural plantations, such as the planting of understorey crops, is recommended for both oil palm and rubber plantations.

Assessment of pollution

Heavy metals, such as Co, Zn, As, Mn, Pb, Cr, Cu, and Ni that pose high ecological risk, were measured to assess the degree of sediment contamination at the Lebir catchment. Long-term exposure to these metals can result in serious health issues both for humans and aquatic species. Continuous monitoring is required for controlling the levels of heavy metals in freshwater environments. The results of I_{geo} are shown in Table 8. The order of mean I_{geo} is as follows: Co > Zn > As > Mn > Pb > Cr > Cu > Ni. The highest contamination and I_{geo} value for Co were recorded in the Lebir Kecil River (4.123), which is categorised as Class 5 (strongly to extremely contaminated). As suggested by Pobi *et al.* (2019), possible causes for the elevated concentration of Co include phosphate fertiliser, disposal of cobalt wastes, and the burning of fossil fuels. These are leads that may lead further focused investigation in this catchment. Cr and Ni were of the lowest contamination level (uncontaminated category) for the studied rivers.

Results for the modified contamination degree (mCd), potential ecological risk index (RI), and background

Table 8 | Results of Igeo

Location	As	Co	Cr	Cu	Mn	Ni	Pb	Zn
Pahi	−0.304	2.605	−1.348	−4.588	−0.343	−3.96	0.969	2.051
Sok	0.209	2.383	−2.285	−3.001	−0.048	0	1.252	2.239
Rek	0.298	2.477	−1.675	−1.639	−0.529	−3.666	0.836	2.347
Sam	0.48	3.088	−1.128	−1.617	−1.282	−3.147	−2.49	1.222
Chalil	1.105	3.674	−3.433	0.761	0.669	0	−3.53	2.718
Miak	0.954	3.628	−1.526	−1.362	0.623	−2.116	−0.568	2.703
Lebir Kecil	0.536	4.123	−0.154	−0.632	0.395	−1.519	−0.189	2.491
Relai	0.333	2.787	−0.459	−1.494	−1.359	−1.9	−2.216	1.034
Aring	2.49	3.169	−0.906	0	5.454	0	−0.382	2.07
Antia	1.167	2.607	−1.022	−2.809	−0.663	−4.091	−0.761	1.9
Koh	0.623	2.895	−0.335	−0.988	−0.91	−2.108	−2.303	1.235
Lebir	0.353	2.884	−0.693	−1.232	−0.538	−2.28	−0.943	1.77
Pertang	0.368	3.119	−1.009	−0.761	0.032	−2.513	−1.28	2.13

enrichment factor (PIN) are presented in Figure 7. The highest mCd value was reported for Aring River (11.992), which was classified as having a 'very high degree of contamination'. The Chalil, Lebir Kecil, and Miak rivers fell under the category of 'high degree of contamination'. mCd values for the Sam, Relai, Antia, Pahi, Sok, Rek, Lebir, Pertang, and Koh rivers, however, were classified as having a 'moderate degree of contamination'. According to the RI, all rivers were at low ecological risk (RI < 150), except for the Aring, Lebir Kecil, Chalil, and Miak rivers (moderate ecological risk; 300 < RI < 150). The PIN pollution index described the Aring River as being contaminated ($518.1 < PIN \leq 2{,}548.6$), whereas other rivers were classified as lightly contaminated ($95.1 < PIN \leq 518.1$) by heavy metals.

The overall results of the pollution indices showed that the Aring River was the most polluted followed by the Lebir Kecil, Chalil, and Miak. Agricultural plantations such as oil palm and rubber have been the major land-use in catchments of these four rivers. Agricultural runoff of chemical fertiliser, insecticides, pesticides, and herbicides may therefore be the cause of the high heavy metal concentrations (Pobi *et al.* 2019). Heavy metal contamination in the Aring River may possibly be due to the high density of oil palm plantations and sand mining activities. Mining in freshwater environments are a major cause of biological and morphological disturbances that could result in the enrichment of heavy metals such as Zn, Mn, Al, Fe, Cr, Cu, and Ni (Pobi *et al.* 2019). Surrounded by HVCF, the Relai River had the least heavy metal contamination within the Lebir catchment. This differs from findings of sediment contribution and erosion rates reported earlier where the logged forest is higher.

CONCLUSION

Based on the chemical signature properties, it is clear that natural environmental conditions in tropical ecosystems are complex – having a melange of tracers not easily distinguishable between sources. However, the combination of chemical analysis, mathematical models, and historical accounts of land-uses has made possible the tracing of non-point-source sediment. Sediment fingerprinting and *in situ* erosion measurements have shown that land disturbances (logging, conversion into agricultural plantations, and mining) are linked to increased erosion and sedimentation, thus affecting the morphology of rivers, and may cause increased flood risk to riverbank areas.

Sediment chemical signatures can be used to calculate various pollution indices as an easy river quality indicator. In this study, the Aring River was the most polluted and may be linked to oil palm plantation and sand mining activities. Immediate implementation of ESCPs is suggested for the studied area.

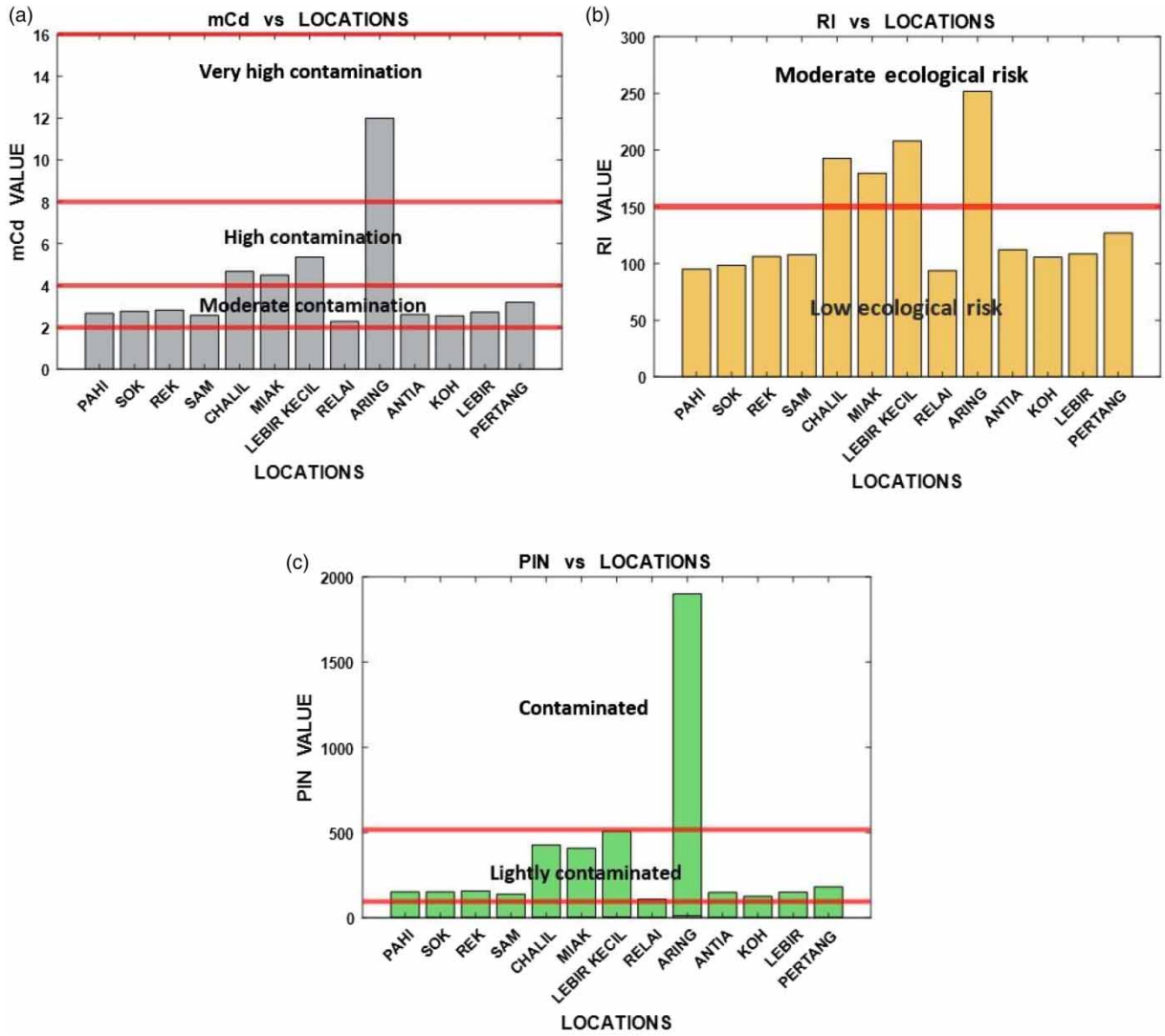

Figure 7 | Sediment pollution indices in the various locations. (a) Modified contamination degree (mCd), (b) potential ecological risk index (RI), and (c) background enrichment factor (PIN).

We have demonstrated that different land-uses result in different erosion and sedimentation characteristics. However, this study is limited in terms of the study period which may result in differences being masked or amplified by within-catchment factors. Similar studies over a longer timeframe and/or utilising more catchments will be beneficial for validation.

ACKNOWLEDGEMENTS

The authors thank the Rasmussen Foundation, United States, for research funds, without which this project would have not been impossible. The authors also express their gratitude to the Forestry Department Peninsular Malaysia (JPSM) and Felda Global Ventures Plantations Sdn Bhd (FGV) for providing research support.

REFERENCES

Abrahim, G. M. S. & Parker, R. J. 2008 Assessment of heavy metal enrichment factors and the degree of contamination in marine sediments from Tamaki Estuary, Auckland, New Zealand. *Environmental Monitoring and Assessment* **136**, 227–238.

Alias, N. E., Mohamad, H., Chin, W. Y. & Yusop, Z. 2016 Rainfall analysis of the Kelantan big yellow flood 2014. *Jurnal Teknologi* **78** (9–4), 83–90.

Annammala, K. V., Walsh, R., Bidin, K. & Nainar, A. 2012 Higher erosion rate and enhanced sedimentation from disturbed landforms in eastern Sabah, Borneo. In: *2nd International Conference on Water Resources in Conjunction with 20th UNESCO-IHP Regional Steering Committee Meeting for Southeast Asia and the Pacific*, Langkawi, Malaysia, 5–9 November 2012, pp. 1–13.

Annammala, K. V., Nainar, A., Yusoff, A. R. M., Yusop, Z., Bidin, K., Walsh, R. P. D., Blake, W. H., Abdullah, F., Sugumaran, D. & Pillay, K. G. 2018 Environmental forensics: a multi-catchment approach to detect origin of sediment featuring two pilot projects in Malaysia. In *Improving Flood Management, Prediction and Monitoring: Case Studies in Asia* (Z. Yusop, A. Aris, N. E. Alias, K. V. Annammala & W. L. Waugh Jr, eds). Emerald Publishing Limited, pp. 49–61.

Caeiro, S., Costa, M., Ramos, T., Fernandes, F., Silveira, N., Coimbra, A., Medeiros, G. & Painho, M. 2005 Assessing heavy metal contamination in Sado Estuary sediment: an index analysis approach. *Ecological Indicators* **5** (2), 151–169.

Clarke, M. A. & Walsh, R. P. D. 2006 Long-term erosion and surface roughness change of rain-forest terrain following selective logging, Danum Valley, Sabah, Malaysia. *Catena* **68** (2–3), 109–123.

Dedkov, A. P. & Gusarov, A. V. 2006 Suspended sediment yield from continents into the World Ocean: spatial and temporal changeability. *Sediment Dynamics and the Morphology of Fluvial Systems*, Vol. 306 (J. S. Rowan, R. W. Duck & A. Werrity, eds). IAHS Publication, Wallingford, pp. 3–11.

Duan, W. L., He, B., Takara, K., Luo, P. P., Nover, D. & Hu, M. C. 2015 Modelling suspended sediment sources and transport in the Ishikari River basin, Japan, using SPARROW. *Hydrology and Earth System Sciences* **19**, 1293–1306.

Hakanson, L. 1980 An ecological risk index for aquatic pollution control a sediment logical approach. *Water Research* **14** (8), 975–1001.

Hydrology and Water Resources Research Laboratory, Kyoto University 2018 Available from: http://hywr.kuciv.kyoto-u.ac.jp/ihp/riverCatalogue/Vol_04/06_Malaysia-3.pdf.

Li, X., Yao, J., Li, Y., Zhang, Q. & Xu, C. Y. 2016 A modelling study of the influences of Yangtze River and local catchment on the development of floods in Poyang Lake, China. *Hydrology Research* **47** (S1), 102–119.

Lim, T. W. 2013 *Malaysia: Illegalities in Forest Clearance for Large-Scale Commercial Plantations*. Forest Trends, Washington, DC. Available from: http://www.forest-trends. rg/documents/index.php.

Luke, S. H., Barclay, H., Bidin, K., Chey, V. K., Ewers, R. M., Foster, W. A., Nainar, A., Pfeifer, M., Reynolds, G., Turner, E. C. & Walsh, R. P. 2017 The effects of catchment and riparian forest quality on stream environmental conditions across a tropical rainforest and oil palm landscape in Malaysian Borneo. *Ecohydrology: Ecosystems, Land and Water Process Interactions, Ecohydrogeomorphology* **10** (4), e1827.

Mohamad, N. A., Jamal, M. H., Annammala, K. V., Yusop, Z., Alias, N. E. & Sugumaran, D. 2018 Impact of forest conversion to agricultural plantation on soil erosion. In *MATEC Web of Conferences*, Vol. 250. EDP Sciences, p. 04004.

MPOB 2020 *Malaysia Palm Oil Board 2018, Monthly Export of oil Palm Products*. Available from: http://bepi.mpob.gov.my/ (accessed March 2020).

Muller, G. 1969 Index of geoaccumulation in sediment of the Rhine River. *GeoJournal* **2**, 108–118.

Nádaská, G., Lesny, J. & Michalík, I. 2010 Environmental aspect of manganese chemistry. *Hungarian Journal Sciences* **100702**, 1–16.

Nainar, A., Bidin, K., Walsh, R. P., Ewers, R. M. & Reynolds, G. 2017 Effects of different land-use on suspended sediment dynamics in Sabah (Malaysian Borneo) – a view at the event and annual timescales. *Hydrological Research Letters* **11** (1), 79–84.

Nainar, A., Tanaka, N., Bidin, K., Annammala, K. V., Ewers, R. M., Reynolds, G. & Walsh, R. P. D. 2018 Hydrological dynamics of tropical streams on a gradient of land-use disturbance and recovery: A multi-catchment experiment. *Journal of Hydrology* **566**, 581–594.

Pejman, A., Nabi Bidhendi, G., Ardestani, M., Saeedi, M. & Baghvand, A. 2015 A new index for assessing heavy metals contamination in sediments: a case study. *Ecological Indicators* **58**, 365–373.

Pobi, K. K., Satpati, S., Dutta, S., Nayek, S., Saha, R. N. & Gupta, S. 2019 Sources evaluation and ecological risk assessment of heavy metals accumulated within a natural stream of Durgapur industrial zone, India, by using multivariate analysis and pollution indices. *Applied Water Science* **9** (3), 1–16.

Tundu, C., Tumbare, M. J. & Kileshye Onema, J. M. 2018 Sedimentation and its impacts/effects on river system and reservoir water quality: case study of Mazowe catchment, Zimbabwe. *Proceedings of the International Association of Hydrological Sciences* **377**, 57–66.

Turekian, K. K. & Wedepohl, K. H. 1961 Distribution of the elements in some major units of the earth's crust. *Geological Society of America Bulletin* **72** (2), 175.

Varol, M. & Bülent, Ş. 2012 Assessment of nutrient and heavy metal contamination in surface water and sediments of the upper Tigris River, Turkey. *Catena* **92**, 1–10.

Walsh, R. P. D., Bidin, K., Blake, W. H., Chappell, N. A., Clarke, M. A., Douglas, I., Ghazali, R., Sayer, A. M., Suhaimi, J., Tych, W. & Annammala, K. V. 2011 Long-term responses of rainforest erosional systems at different spatial scales to selective logging and climatic change. *Philosophical Transactions of the Royal Society B: Biological Sciences* **366** (1582), 3340–3353.

First received 31 July 2019; accepted in revised form 1 May 2020. Available online 10 June 2020